Total Lightning Information in a 5-Year Thunderstorm Climatology

Benjamin S. Herzog[1,2,*], Kristin M. Calhoun[1,2], and Donald R. MacGorman[2]

[1]Universtiy of Oklahoma/Cooperative Institute for Mesoscale Meteorological Studies (CIMMS), Norman, Oklahoma, U.S.A.
[2]NOAA/OAR/National Severe Storms Laboratory (NSSL), Norman, Oklahoma, U.S.A.

ABSTRACT: Total lightning information has been shown to be proportional to storm intensity. While this relationship is currently only useful in the few regions with access to total lightning information, the Geostationary Lightning Mapper (GLM), which will be on-board the Geostationary Operational Environmental Satellite-R series (GOES-R) satellite, will provide total lightning information across the contiguous United States. This information will be available at a temporal resolution of 1 minute, thus providing a proxy of storm strength that will be available more frequently than traditional measures of storm intensity. In an effort to increase the value of the information that will be provided by the GLM, the goal of this study is to enhance the understanding of total lightning information by exploring it in the framework of a 5-year climatology. In this study, total lightning information is examined across 3 different geographic domains (Central Oklahoma, Northern Alabama, and Washington, D.C.), with each domain corresponding to the location of a lightning mapping array. Specifically, this research; a) determines how total lightning attributes of thunderstorms vary between different geographic regions, b) examines relationships between total lightning attributes and radar-derived attributes in thunderstorms, and c) determines how total lightning attributes vary between hazardous and non-hazardous storms.

INTRODUCTION

Previous studies have shown that the relationship between the updraft and lightning production can be exploited to both improve the output of numerical models by assimilating lightning data [e.g., *Mansell et al.*, 2007] and to improve the warning capability of the human forecaster by supplementing traditional means of accessing storm intensity (e.g., the WSR-88D network, e.g., *Darden et al.* [2010]). Unfortunately, these potential benefits from total lightning information currently apply only to the few areas with access to total lightning data via networks such as the lightning mapping array (LMA). However, the Geostationary Lightning Mapper (GLM), which will be on board the Geostationary Operational Environmental Satellite-R series (GOES-R) satellite, will provide total lightning information across the contiguous United States (CONUS, *Goodman et al.* [2006]). Therefore, once the GLM is operational, a means to access total lightning, and thus estimate storm intensity, will be available across much of the North American continent, including traditionally data-sparse regions such as mountainous areas and oceans. Furthermore, this information will be available at a temporal resolution of 1 minute, thus providing a measure of storm intensity that will be available more frequently than traditional measures of storm intensity.

While there have been many studies that have examined relationships between lightning activity and single polarization radar variables [e.g., *Lhermitte and Krehbiel*, 1979; *MacGorman et al.*, 1989; *Emersic et al.*, 2011], polarametric radar variables [e.g., *Carey and Rutledge*, 1996; *Petersen et al.*, 2005; *Calhoun et al.*, 2013], and storm intensity [e.g., *Goodman et al.*, 1988; *Williams et al.*, 1999; *Schultz et al.*, 2011], there have been relatively few studies aimed at exploring these relationships in the framework of a multi-year climatology. Therefore, the goal of this study is to examine total lightning information over a period of

*Corresponding author, email: benjamin.herzog@noaa.gov, Postal address: NSSL, 120 D. L. Boren Blvd., Norman, OK 73072 U.S.A.

5 years. This information is examined across 3 different geographic domains (Central Oklahoma, Northern Alabama, and Washington, D.C.), with each domain corresponding to the location of an LMA network. Specifically, this research will; a) examine the climatological characteristics of total lightning information, b) examine relationships between lightning characteristics and radar derived storm attributes in thunderstorms, and c) determine how lightning characteristics vary between hazardous and non-hazardous thunderstorms. Through the examination of these relationships over a period of several years, we will be capable of more accurately understanding and harnessing total lightning information, thus greatly improving the value of the information available from the GLM.

DATA AND METHODS

To examine total lightning characteristics of thunderstorms in the framework of a multi-year climatology, a method that automatically identified thunderstorms and tracked various attributes associated with the storms was developed. This methodology required the use of data from multiple sources. Due to the large quantity of data that was utilized in this study, it was necessary to implement automated algorithms to perform data processing. Most of the algorithms used in this study are a part of the Warning Decision Support System-Integrated Information (WDSS-II) software. WDSS-II contains a suite of automated algorithms capable of visualizing, analyzing, and quality-controlling a variety of meteorological datasets [*Lakshmanan et al.*, 2007b].

Data from each source was packaged in 24-hour periods and processed in parallel through the use of the Boomer Supercomputer at the University of Oklahoma. Once the data from the individual data sources were processed, they were then ingested into WDSS-II multi-radar/multi-sensor (MRMS) algorithms. The MRMS algorithms combined the individual datasets into a set of grids for each domain and eventually resulted in observations of every storm in each domain at a temporal resolution of 1 minute. For this study, the primary data sources were 3 lightning mapping arrays (LMAs), 24 Weather Surveillance Radar-1988 Doppler (WSR-88D) radars, and the Rapid Update Cycle (RUC, *Benjamin et al.* [2004] numerical forecast model. Only data within 125 km of the LMA network centers were considered. These domains are shown in Fig 1.
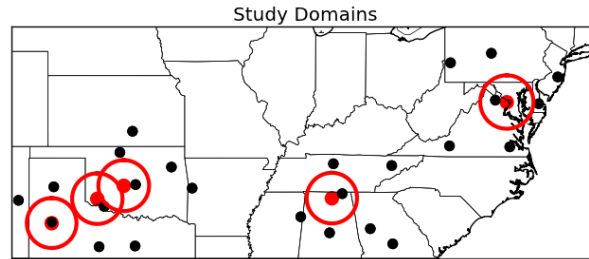

Figure 1: The domains examined in this study. Shown are the WSR-88D radar sites (black dots), LMA network centers (red dots), and domains (red circles).

The LMAs utilized in this study were the Washington D.C. LMA (DCLMA, *Krehbiel* [2008]), the Northern Alabama LMA (NALMA, *Goodman et al.* [2005]), the Central Oklahoma LMA (OKLMA, *Krehbiel et al.* [2000]; *MacGorman et al.* [2008]), and for the final 8 months of 2012, the West Texas LMA (WTLMA, *Bruning* [2012]). Each array detects the VHF lightning sources emitted by lightning flashes. Since a given lightning discharge may produce tens to several thousand sources, the individual sources identified by the LMAs were sorted into flashes based on criteria in time as space, as describe in *MacGorman et al.* [2008]. Once the sources were grouped into individual flashes, the composite flash extent density

(FED) and composite flash initiation density (FID) products were also produced with a spatial resolution of 1 km x 1 km and a 1 minute temporal resolution. The FED is defined as the number of lightning flashes contained in a grid box. The FID is defined as the location of the origin of a flash, and is computed according to an algorithm described in *Lund et al.* [2009]. Schematics of these products are provided in Figure 2.

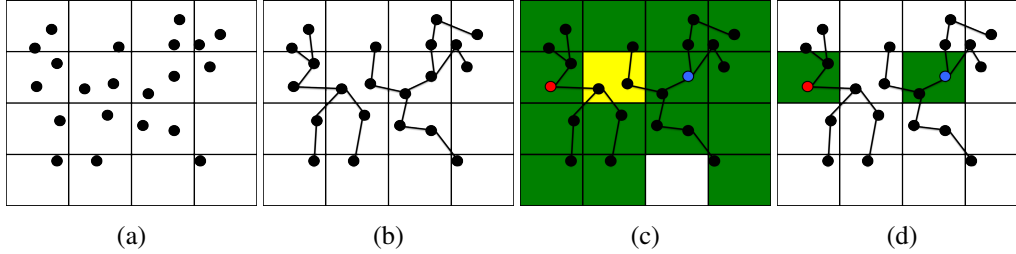| (a) | (b) | (c) | (d) |

Figure 2: A schematic of a) raw LMA sources, b) LMA sources grouped into flashes, c) flash extent density, and d) flash initiation density.

Once the LMA data were processed, data from the individual WSR-88D were first quality controlled with a neural network ([*Lakshmanan et al.*, 2007a]) and then dealiased with a technique that solves a two dimensional least squares problem in order to determine correction values for all range gates [*Jing and Weiner*, 1993]. Finally, an algorithm that implemented a local, linear least squares (LLSD) method to compute the rotational derivative of radial velocity was used to obtain the azimuthal shear from 0-2 km above ground level (AGL) (low-level shear) and from 3-6 km AGL (mid-level shear) [*Smith and Elmore*, 2004].

After the data from the individual radars were processed, the data from all radars in each domain were merged to create a 3-dimensional cube of reflectivity data, a grid of composite reflectivity, as well as 2 grids of azimuthal shear (0-2 and 3-6 km above AGL) over each domain. This was accomplished through the use of an algorithm that accounted for varying radar beam geometry with range, vertical gaps between radar scans, the lack of time synchronization between radars, storm movement, varying beam resolutions between different types of radars, beam blockage due to terrain, differing radar calibration, and inaccurate time stamps on radar data [*Lakshmanan et al.*, 2006]. Additionally, by integrating the RUC information with the merged radar data, several fields of derived radar products were created in this step.

The final step was to automatically identify thunderstorms and track the attributes associated with each storm. The identification and tracking of storm clusters was achieved through the use of the WDSS-II algorithm w2segmotionll (segmentation and motion estimation on a latitude-longitude grid, *Lakshmanan et al.* [2003]; *Lakshmanan and Smith* [2009]). This algorithm used a combination of K-means clustering and enhanced watershed segmentation to first simplify the grid of interest and then determine the spatial extent of storms. These identified storms, or clusters, were identified at multiple spatial scales (100, 500, 1000, and 2000 km^2). Once identified, the clusters in each scale were matched in time by determining the movement that minimizes the mean absolute error between the current frame and the corresponding pixels in the previous frame [*Lakshmanan et al.*, 2003]. The clusters that are matched through this movement are then identified as the same storm.

The size of the clusters identified at each scale did not deviate much from the size defining the scale, except for the largest scale, whose clusters grew unbounded (because the clusters at the largest scale grew unbounded, these clusters were not included in the analysis presented herein). Therefore, the smallest scale performed fairly well in identifying and tracking storms around 100 km^2, but was only able to identify the core of larger storms. Inversely, the larger scales did not identify storms that were smaller than the scale size,

but were capable of tracking larger portions of the storms once they became large enough to be identified. This discrepancy was a problem in two situations: when there were multiple storms that could only be identified with different scales, and when a storm transitioned from being identified at one scale to being identified at the other.

With these issues in mind, an algorithm was developed that would ingest clusters at all scales and ultimately determine the clusters that optimally identify the storms. This algorithm simply takes the clusters identified with w2segmotionll at every scale and flattens them down to one image. If a storm is identified at multiple scales, only the cluster at largest scale the storm is identified at is used. The output of this flattening algorithm provides more complete storm tracking than the aforementioned capability to identify storms at multiple scales while only counting the attributes from each storm once. An example of the output from the flattening algorithm is given in Fig. 3.
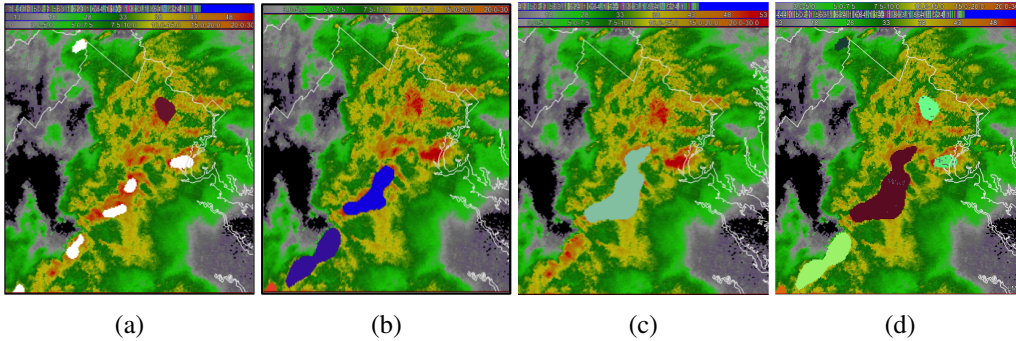

| (a) | (b) | (c) | (d) |

Figure 3: Figs. a, b, and c show the storms identified by w2segmotionll at scales 0, 1, and 2 respectively. Fig. d is the result of the flattening algorithm on the images in a, b, and c. The solid colored clusters represent storms identified. The dots in the clusters are the flash initiation points.

Finally, a storm type was automatically assigned to each storm identified with w2segmotionll. The storm type was determined through the use of the automated storm typing algorithm described in *Hobson et al.* [2012]. This algorithm used a decision tree to classify storms as supercells, ordinary, and short-lived. The storm type classification decision tree (Fig. 4) was obtained through the automated analysis of thousands of storms and is not subjective.

RESULTS

The storm identification and tracking described above resulted in one minute observations of every identified storm that occurred in each domain over the five year period. Each one of these observations contained information about several total lightning and radar-derived attributes. For a given observation, these attributes were obtained through examination of each total lightning and radar-derived field in all pixels of the identified storms. In total, the data contained several million of these thunderstorm observations. However, the number of observations used in this analysis was actually much smaller than the total size of the dataset. Any storm observations that were not completely within 125km of an LMA network center were not considered. Also, there were many instances where an identified storm failed to produce lightning at any point in its lifetime; observations from non-electrified storms were thrown out. Finally, observations from any storm that lasted less than 30 minutes were also not considered.

After these quality control measures were taken, the resulting data included 1,094,728 thunderstorm observations. To assure data independence, the data were then sampled according to the longest average decorrelation time (DCT) of all attributes. The DCT was found by determining the lag at which the auto-
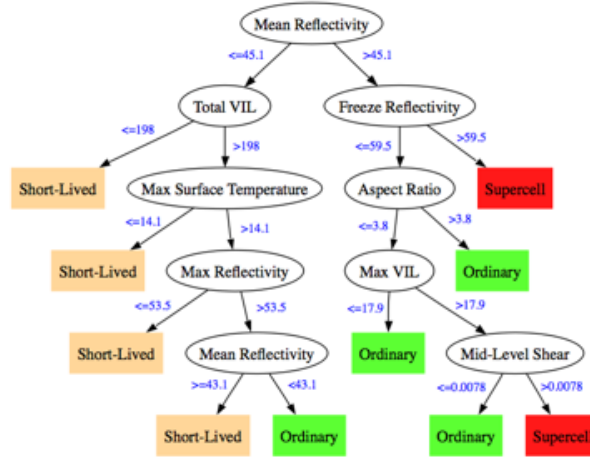
Figure 4: From *Hobson et al.* [2012], the decision tree used to classify the type of each storm.

correlation function fell below 1/e for each attribute [*Rudlosky and Fuelberg*, 2013]. The longest average DCTs were between 9 and 10 lags; thus the set of 1,094,782 observations was sampled every 10 minutes. This sampling resulted in 106,327 thunderstorm observations, and each observation contained values for every total lightning and radar-derived attribute. Of the 106,327 total observations, 24,993, or about 24 percent, were from the DCLMA, 45,052, or about 42 percent, were from the NALMA, and 36,282, or about 34 percent, were from the OKLMA.

The total lightning attributes examined in this study are the total flash rate (TFR), the normalized flash density (NFD), the mean flash extent density (Mean FED), and the maximum flash extent density (Max FED). The TFR is the number flash initiation points in each storm observation. Since a storm observation was taken every minute, the flash count for an observation is given in flashes per minute (fpm) and is called the TFR. In an attempt to normalize for storm size, the TFR was divided by the area of the identified storm cluster to produce NFD. The FED is the number of distinct lightning flashes traversing a grid cell. Since each grid had a horizontal resolution of 1 km x 1 km, the unit for FED is channels km^{-1}. The Mean FED is computed by calculating the mean FED value from all pixels in each identified storm Finally, the Max FED is the highest FED value in any pixel in the storm at the observation time.

To examine the differences and similarities in these attributes, the Pearson's and Spearman's correlation coefficient between each pair of total lightning attributes was computed (Table 1). For each pair of attributes, the Pearsons correlation exceeded 0.66, implying a moderately strong, direct linear relationship. Furthermore, the Spearman's correlation, which is a non-parametric measure of strength of relationship, exceeded 0.86 for all pairs of attributes, indicating that the relationship is strong between each of these attributes, and that there are also some non-linearities in these relationships.

Due to the strength of relationship among each of these attributes, the remainder of this paper will focus primarily on only one of the total lightning attributes, the Max FED. Max FED was chosen because it displayed the highest correlation with each of the other attributes. Additionally, because the maximum in FED typically occurs near the storm center, the storm tracking algorithm is less likely to miss the actual maximum in FED than it is to miss lightning flashes occurring on the periphery of storms.

Climatological Characteristics

1. *Total Flash Count* The number of independent 1-minute observations and total lightning flashes observed in each domain are given in Table 2. The number of flashes observed by the DCLMA was

Table 1: The Pearson's (lower left) and Spearman's (upper right) correlation coefficients among the total lightning attributes explored.

	Flash Rate	NFD	Mean FED	Max FED
Flash Rate		0.97	0.87	0.92
NFD	0.67		0.88	0.90
Mean FED	0.72	0.82		0.96
Max FED	0.83	0.73	0.82	

around one third of the amount of flashes observed in the other domains. While the number of flashes observed in the OKLMA and NALMA were roughly equal, the flashes observed in the OKLMA domain occurred in approximately 20 percent fewer observations than in the NALMA, showing that on average, observations from the OKLMA had more flashes than in the NALMA.

Table 2: The total number of observations and flashes from the observations in each domain.

	Total	DCLMA	NALMA	OKLMA
Observations	106,327	24,993	45,052	36,282
Flashes	787,923	138,357	313,965	335,601

The temporal variations in total flash count for each domain are shown in Fig. 5. In the month-to-month variations of total flash count (Fig. 5a), the total lightning production was maximized during the warm season. In all but 4 months (March, June, July, December), the OKLMA produced more total lightning flashes than the other domains, while the DCLMA produced the least amount of lightning in all months.

In addition, the hourly variations in total flash count (Fig. 5b) reveal a diurnal pattern in total lightning production. The total lightning count was maximized in the afternoon to early evening hours prior to a lull in the overnight to morning hours. Additionally, the peak in total flash count in the NALMA occurred before the peak in the DCLMA by approximately 1-2 hours. This peak in the DCLMA preceded the peak in the OKLMA by approximately 1-2 hours. Finally, the peak in the OKLMA tailed off much more slowly than the peak in the other domains.

2. *Maximum Flash Extent Density* The distributions of Max FED for each of the domains are shown in Fig. 6. Summary statistics (the median, first quartile ($q_{.25}$), third quartile ($q_{.75}$), mean, standard deviation, and maximum) for these distributions are provided in Table 3. The values in Table 3 represent the 95 percent confidence interval for each statistic obtained through bootstrapping the observations 5,000 times. Additionally, to test if the differences in the statistics between the domains were significant at the 0.05 level, permutation tests were performed. The p-values from these tests were obtained by permuting the dataset 10,000 times. When statistical significance is discussed, it is in reference to these tests.

Clearly, these distributions were highly skewed. The median value in each domain was 1.0, indicating that at least half of the 1-minute observations had a Max FED of 1 or 0. The range of the Max FED
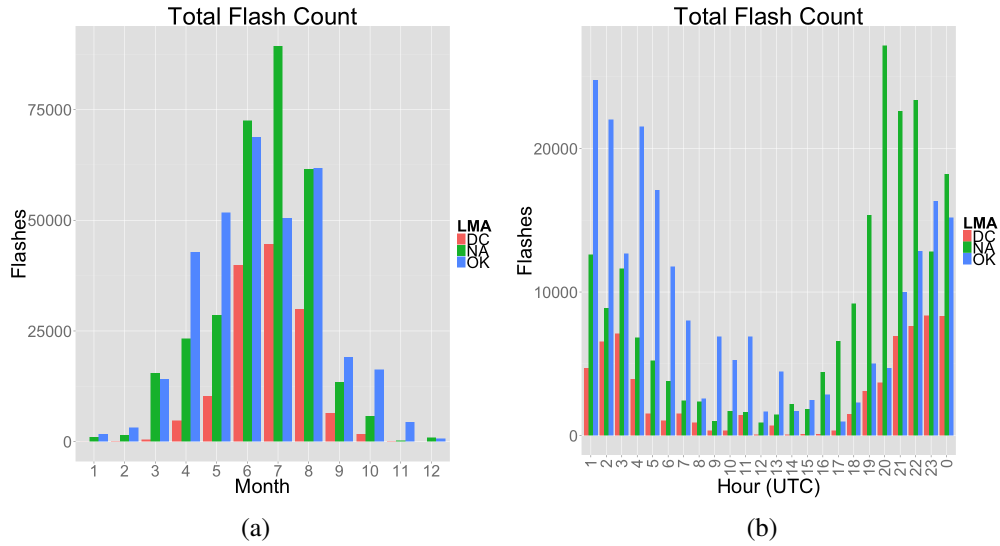
Figure 5: The temporal variation in the total flash count for each domain.

Table 3: The 95 percent confidence intervals for summary statistics of Max FED.

	DCLMA	NALMA	OKLMA
Median	1.0-2.0	1.0-1.0	1.0-1.0
$q_{.25}$	0.0-0.0	0.0-0.0	0.0-0.0
$q_{.75}$	3.0-4.0	5.0-5.0	5.0-5.0
Mean	3.04-3.18	4.20-4.34	5.41-5.64
SD	5.67-6.00	7.70-7.98	10.64-11.07
Max	70.0-85.0	70.0-72.0	93.0-105.0

then extended well beyond $q_{.75}$. The inter-quartile ranges (IQR, $q_{.75} - q_{.25}$) in each of the domains were quite similar to one another, with the only significant difference being that $q_{.75}$ was lower in the DCLMA than in the other domains. The mean value for each distribution was also computed. Here, the mean values in the OKLMA exceeded the mean values in the NALMA, the mean values in the NALMA exceeded the mean values in the DCLMA, and these differences are statistically significant.

Next, the temporal variations of Max FED were examined. To do this, the central location of the Max FED in all domains was computed for each month and hour. Typically, when dealing with highly non-Gaussian data, the median is the preferred measurement of central tendency. The median is a robust and resistant statistic that is ideal for exploring highly skewed datasets. However, because over half of the observations had a Max FED of either zero or one, the median revealed little useful information. Rather than using a measure of central tendency that is not well suited to non-Gaussian distributions, such as the mean, all observations of zero TFR were dropped in order for the median to still be used to characterize the data. For the sake of completeness, the distributions and summary statistics for the zero-removed distributions are provided in Fig. 7 and Table 4.

By removing observations of 0 TFR, the median value in each domain was slightly increased and
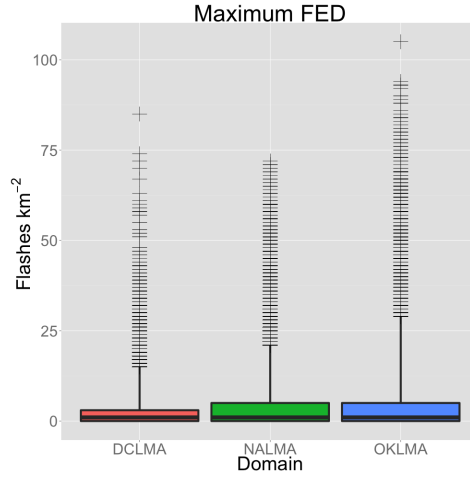
7

Figure 6: Distributions of Max FED in each of the domains. The boxes represent the IQR and the whiskers extend to the 5th and 95th percentile of observations. Observations outside of the 5th and 95th percentile are represented by crosses.
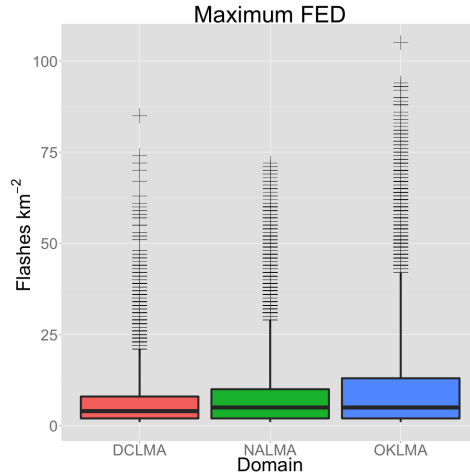

Figure 7: As in Fig. 6, but with observations of 0 TFR removed.

there was a significant difference in the median of the DCLMA and the other domains. Additionally, all other statistics in each domain, barring $q_{.25}$ and the maximum, were significantly different when observations of 0 TFR were dropped. Furthermore, for most statistics, the value in the OKLMA exceeded the value in the NALMA, and the value NALMA exceeds the value in the DCLMA. The month-to-month variability of the median Max FED is shown in Fig. 8a. Unsurprisingly, the median Max FED in the summer months tended to be larger than those in the cool season for all domains. The month-to-month variations show that the median TFR from the OKLMA was at least as high as the median TFR from the other domains in all months but July. Inversely, the median Max FED in the DCLMA was never higher than the median Max FED from the other domains.

Examination of the hour-to-hour variations (Fig. 8b) revealed the same diurnal trend in the median Max FED that was found when looking at the total number of flashes. For each domain, the median

Table 4: The 95 percent confidence intervals for summary statistics of Max FED with all observations of zero TFR removed.

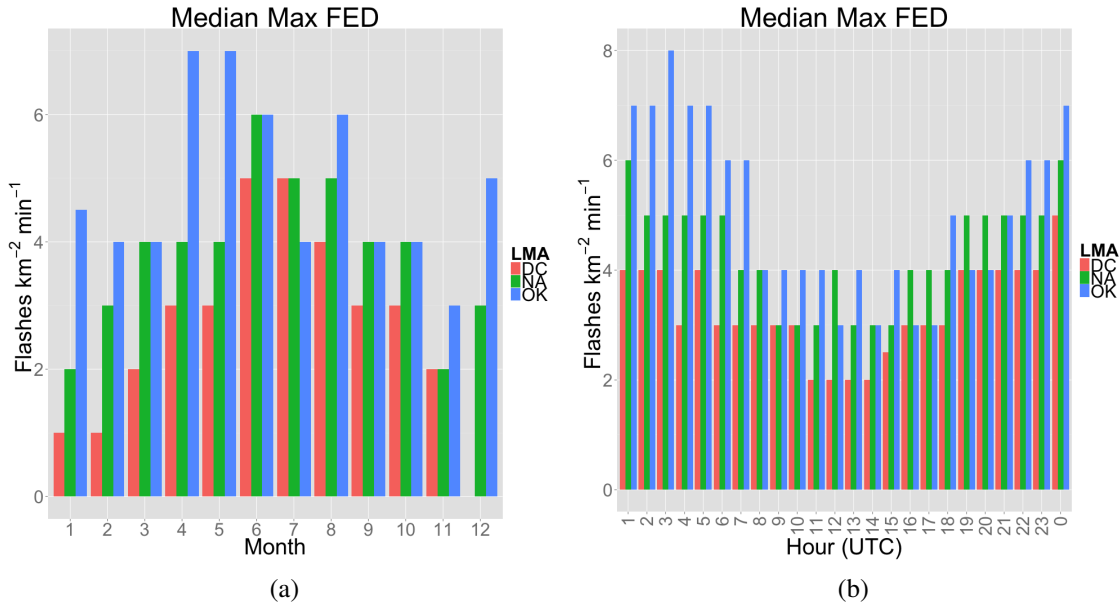|	DCLMA	NALMA	OKLMA
Median	3.0-3.0	3.0-4.0	4.0-4.0
$q_{.25}$	2.0-2.0	2.0-2.0	2.0-2.0
$q_{.75}$	6.0-7.0	8.0-9.0	10.0-11.0
Mean	5.42-5.65	6.99-7.21	9.03-9.36
SD	6.64-7.09	8.89-9.23	12.49-13.00
Max	70.0-85.0	70.0-72.0	93.0-105.0

Figure 8: Month-by-month and hour-by-hour variations of Max FED.

Max FED was maximized in the late afternoon or evening, and there was a lull in the morning. The peak in median Max FED occurred at 0z, 0z and 3z for the DCLMA, NALMA, and OKLMA, respectively. In all but 5 hours (12, 16, 17, 19, and 20 UTC), the median value of max FED in the OKLMA was at least as great the median value of max FED in the other domains.

Attribute Comparison

In an effort to contextualize the total lightning thunderstorm attributes in terms of thunderstorm characteristics already understood by forecasters, the relationships between the total lightning and radar-derived thunderstorm attributes were examined. A large number of radar-derived attributes were examined, and a sample of those radar-derived attributes are explored here. To start, simple correlation coefficients were examined. As was done earlier in this section, both the Pearson's (p) and Spearman's (s) correlation coefficient were computed (Tables 5 and 6) for several pairs of attributes. The majority of the attribute pairs had a p greater than 0.50, which implies a moderate linear relationship, and 2 of the attribute pairs had a p greater

than 0.70, which implies a strong linear relationship between these variable pairs.

Table 5: The Pearson's correlation coefficient between total lightning attributes and a selection of the radar-derived attributes examined in this study

| | Pearson's Correlation | | | |
	Flash Rate	NFD	Mean FED	Max FED
Mean Reflectivity	0.41	0.47	0.54	0.44
Max Reflectivity	0.37	0.35	0.39	0.46
Area > 40 dBZ at -10C	0.76	0.44	0.58	0.62
Max Reflectivity at -20C	0.49	0.49	0.50	0.60
40 dBZ Echo Tops	0.56	0.53	0.53	0.63
Max VII	0.64	0.58	0.59	0.71
MESH	0.63	0.54	0.55	0.66
Max Low Level Shear	0.44	0.29	0.38	0.43

Table 6: The Spearman's correlation coefficient between total lightning attributes and a selection of the radar-derived attributes examined in this study

| | Spearman's Correlation | | | |
	Flash Rate	NFD	Mean FED	Max FED
Mean Reflectivity	0.46	0.48	0.53	0.49
Max Reflectivity	0.66	0.62	0.62	0.67
Area > 40 dBZ at -10C	0.75	0.70	0.70	0.75
Max Reflectivity at -20C	0.72	0.70	0.69	0.74
40 dBZ Echo Tops	0.68	0.65	0.63	0.68
Max VII	0.71	0.68	0.66	0.72
MESH	0.66	0.63	0.57	0.66
Max Low Level Shear	0.47	0.40	0.41	0.47

As discussed previously, the distributions for all total lightning attributes were highly skewed, and therefore the non-parametric s would be expected to give a more meaningful measure of the strength of relationship between pairs of attributes than p. Indeed, in nearly every pair of lightning and radar-derived attributes, s exceeded p. For nearly all pairs of variables, s exceeded 0.50, and in 9 of the attribute pairs show, exceeded 0.70.

A subset of the radar-derived attributes compared above was chosen to examine the relationships with the total lightning attributes in greater depth. The specific attributes discussed below were selected to present a variety of radar attributes, as well as to examine more closely the pairs of attributes that displayed the highest correlation coefficients. The chosen radar-derived attributes were: the area of reflectivity at -10 C greater than 40 dBZ (-10RefGT40), the maximum reflectivity at -20 C (-20MaxRef), the maximum 40 dBZ echo tops (ET40), and the maximum vertically integrated ice (MaxVII). p between these attributes and Max FED for each of the above pairs of attributes was 0.62, 0.60, 0.63, 0.71, respectfully. In each of these

pairs of attributes, s was nearly the same or greater than p, thus revealing that the relationship between these pairs of attributes may not have been linear. The nature of these relationships can be further diagnosed upon the examination of the scatterplots (Fig. 9).

In the scatterplot between Max FED and -10RefGT40 (Fig. 9a), a large portion of the observations occurred when the -10RefGT40 was small relative to the maximum value of -10RefGT40. This implies that like the Max FED, the distribution of -10RefGT40 was also skewed. Additionally, we see in this plot that the very largest total lightning values occurred only when the -10RefGT40 was less than about 1000 square km. The scatterplot between Max FED and -20MaxRef was quite a bit different (Fig. 9b). The distribution of -20MaxRef was closer to normal than that of -10RefGT40. Additionally, the largest values of Max FED only occurred when -20MaxRef was also large. A similar pattern was clear when examining Max FED and ET40 (Fig. 9c), although ET40 has a less normal distribution than -20MaxRef. Finally, the scatterplot between Max FED and Max VII (Fig. 9d) showed that like -10RefGT40, Max VII had a skewed distribution. However, unlike -10RefGT40, the largest values of Max FED occurred when the Max VII was large.

Hazard Recognition

Finally, we examine the usefulness of total lightning information in the discrimination of hazardous and non-hazardous thunderstorms. Previous research has shown that total lightning information may be able to delineate between severe and non-severe storms [e.g., *MacGorman et al.*, 1989; *Williams et al.*, 1999]. However, these studies utilized severe weather reports from NCDC's StormData. The majority of severe weather reports in StormData come from the general public, which results in significant inconsistencies due to the subjective nature of this reporting. Furthermore, a large portion of severe weather goes unreported due to the fact that it occurs in unpopulated areas where human observation is rare.

Therefore, in order to capture a larger fraction of severe thunderstorms than what can be identified by severe weather reports alone, an automated storm typing algorithm [*Hobson et al.*, 2012] was implemented to identify supercell thunderstorms, which have been shown to produce a disproportionate amount of severe weather [e.g., *Doswell and Burgess*, 1993; *Moller et al.*, 1994]. Through the use of the storm typing algorithm, storms that are known to frequently produce severe weather are objectively and consistently identified at all locations in each domain. Once the supercell thunderstorms were identified, the total lightning attributes of hazardous (supercell) and non-hazardous (non-supercell) thunderstorms were examined. This algorithm classified storms as supercell or non-supercell at each minute, meaning that a particular storm may change storm type from minute to minute.

Rather than simply identifying entire storms as severe or non-severe, we have instead chosen to isolate the hazardous portions of thunderstorms. To do this, only the observations directly classified as supercells by the storm typing algorithm were considered supercells. Of the 106,327 total observations, 3852 were identified as supercells. Of the supercell observations, 2327 observations (approximately 60 percent) came from storms that produced severe weather according to StormData. It is likely that a larger portion of these observations actually produced severe weather, but went unreported.

The distributions of Max FED in non-supercell and supercell observations are given in Fig. 10. Clearly, there is a difference in these distributions. In fact the median Max FED in supercell observations was approximately 20 channels km^{-2} larger than in non-supercell observation. Furthermore, there was zero overlap in the IQR of these distributions. While significance testing was not done on these distributions, these observations indicate the differences in these distributions are likely statistically significant.
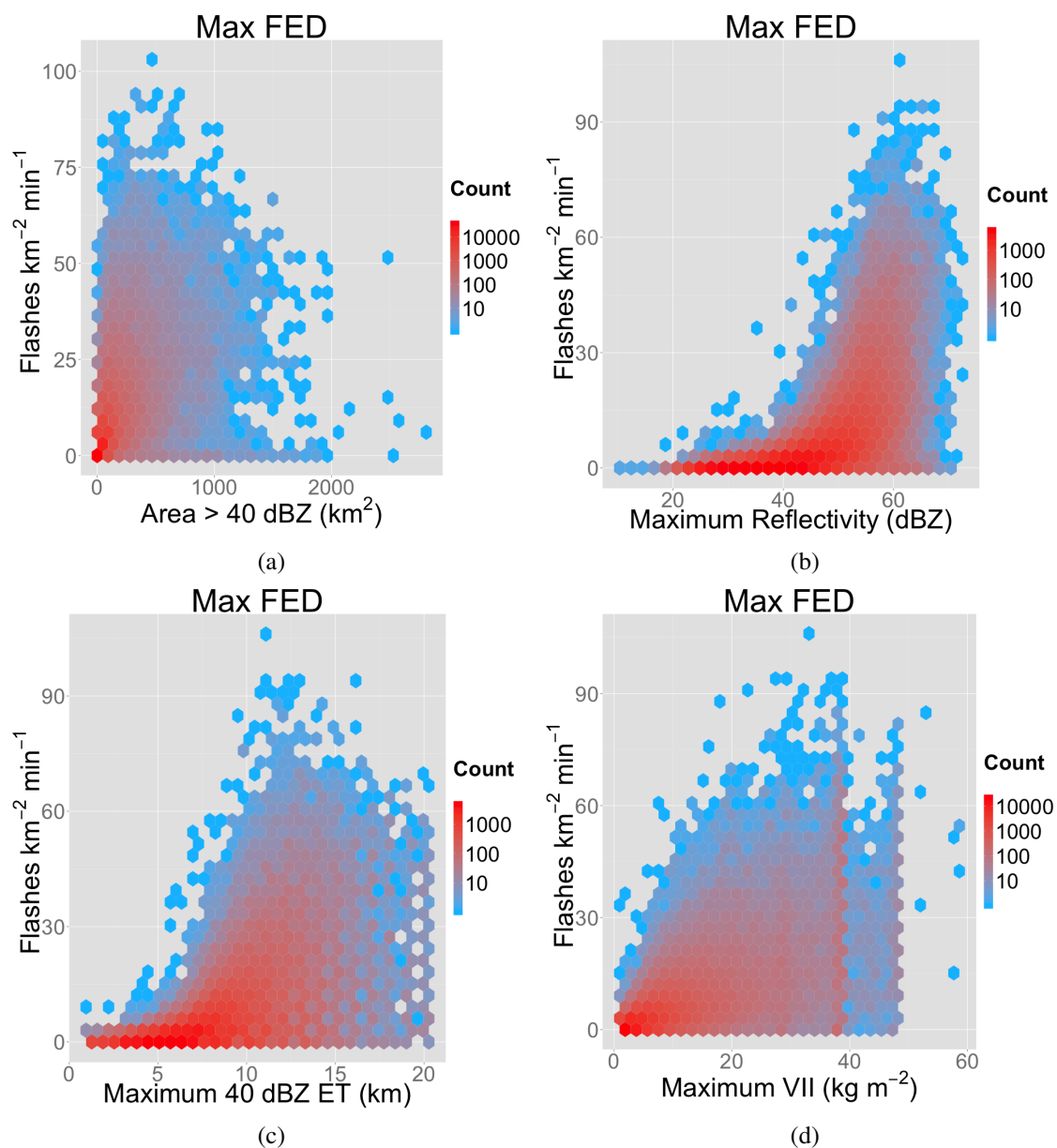
11

Figure 9: Scatterplots of Max FED and: a) Area of reflectivity greater than 40 dBZ at -10 C, b) Maximum Reflectivity at -20 C, c) Maximum 40 dBZ echo tops, and d) Maximum VII.
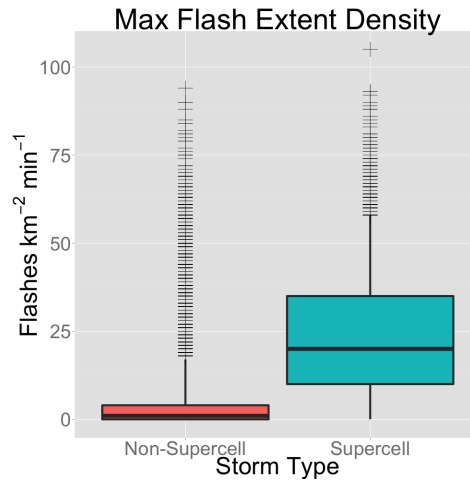
Figure 10: The distribution of Max FED in hazardous and non-hazardous storms

DISCUSSION

Climatological Characteristics

Several patterns were identified through the examination of the climatological characteristics of total lightning attributes. First of all, the total number of flashes, along with the median values of each total lightning attribute, were maximized in the warm season, coincident with the annual peak in convective activity [e.g., *Long*, 1966; *Kelly et al.*, 1985]. Not only are storms more numerous in the warm season, but the convective activity in the spring and summer months also tends to be more vigorous than in other months, meaning that storms occurring in those months are capable of separating more charge [*Lhermitte and Williams*, 1983; *Dye et al.*, 1986; *Williams et al.*, 1989], thus resulting in larger median values for each total lightning attribute.

The diurnal variation in the total number of flashes and in the median value of each total lightning attribute each exhibited a maximum in the late afternoon to early evening hours. Typically, convective activity is maximized during the late afternoon and early evening in conjunction with the peak solar heating [e.g., *Easterling and Robinson*, 1985; *Kelly et al.*, 1985], thus causing the total number of flashes to be maximized. Additionally, storms occurring in the late afternoon to early evening typically have larger updrafts with increased mass flux separating more charge and initiating more lightning, thus resulting in higher median values of the total lightning attributes.

The median value of the total lightning attributes during each hour was the greatest in the OKLMA and least in the DCLMA. However, from approximately 16 UTC to 20 UTC, the median values of the total lightning attributes in the NALMA, and in some cases the DCLMA, were comparable or greater than in the OKLMA. This is because the time of peak convective activity in the NALMA and DCLMA occurs earlier in the UTC reference day than in the OKLMA. The OKLMA is farther west than the other domains, and so the peak heating occurs at a later time, thereby causing the lightning activity to be maximized later in UTC time. Finally, the median values of the total lightning attributes in the OKLMA remained elevated after the peak in activity longer into the overnight hours than they did in the other domains. This can likely be attributed primarily to the mesoscale convective systems (MCS) that frequently occur in the central U.S. in the spring and summer months [*Maddox*, 1980]. These MCSs typically occur during the overnight to early morning hours, last for several hours, and can produce a substantial amount of lightning [e.g., *Goodman and MacGorman*, 1986; *Lund et al.*, 2009; *Makowski et al.*, 2013].

13

In the examination of the overall distributions of the observations of total lightning attributes, most of the summary statistics indicated that in general, observations in the OKLMA contained higher values of total lightning attributes than observations in the NALMA, and observations in the NALMA contained higher values of the total lightning attributes than observations in the DCLMA, with only a few exceptions. This pattern was especially clear when examining the mean values of each attribute, and when examining the distributions for which the observations of zero lightning were omitted. In all cases, the difference in the means of the total lightning attributes between domains were greater than the difference in the medians. This happens because the mean is more heavily influenced by long tails, such as the tails found in the distributions of each of these attributes. While there is little difference in the bottom half of these distributions (indicated by similar or identical medians), the difference in total lightning activity between the domains increases when the total lightning attributes are larger than the median. In other words, as the electrical activity in a storms increased beyond the medain, storms in the OKLMA were more electrified than storms in the NALMA, and storms in the NALMA were more electrified than storms in the DCLMA.

Attribute Comparison

Both the Pearson's and Spearman's correlation coefficients were computed for several pairs of total lightning and radar-derived attributes, revealing a direct, moderate to strong relationship between many of the attribute pairs. This is consistent with previous studies by *Lhermitte and Krehbiel* [1979], who found that storm electrification in a Florida thunderstorm was closely related to substantial radar reflectivity, *Mazur* [1989], who found a positive correlation between maximum lightning density and the 40 and 50 dBZ echo top heights in a thunderstorm in Virginia, and *Rudlosky and Fuelberg* [2013], who found correlation coefficients similar to the correlation coefficients discussed here between some of the total lightning and radar-derived attributes examined in this research.

This relationship between the total lightning and radar-derived attributes exists because of a storm's updraft. The updraft of a storm has a direct effect on how much lightning is produced. As the updraft volume or updraft mass flux is increased, more particles interact to separate charge and the charged particles are separated more quickly, thus initiating lightning more frequently [e.g., *Lhermitte and Williams*, 1983; *Williams*, 1989]. Likewise, when the updraft in a storm is stronger, nearly all of the radar-derived attributes discussed in this paper are also enhanced. Therefore, since both the total lightning and radar-derived attributes are at least partially governed by the updraft, there is a strong relationship between them.

1. *Forecast Applications* Due to the strength of the relationships between the total lightning and radar-derived attributes, a natural offshoot is to attempt to make predictions of one based on the other. Predictions can be made by establishing what levels of radar-derived and total lightning attributes occurred coincidently in the past, and extending these relationships into the future. Predictions of radar-derived attributes based off of total lightning attributes may be of particular use to a forecaster in an operational setting due to the enhanced temporal resolution of the total lightning information. By showing what level of radar-derived attribute can be expected based on the total lightning information, forecasters can then use their understanding of how the radar derived attributes relate to storm intensity to create a link between total lightning information and storm intensity.

   To determine what levels of radar-derived attributes occur when different total lightning thresholds are observed, the total lightning attributes were broken up into six bins and all observations were sorted into these bins. The first bin was defined to contain observations in which the lightning attribute was zero and the last bin was defined to contain observations for which the value of the lightning attribute was in approximately the upper one percent of total lightning observations. The remaining four bins

were chosen in an attempt to balance bin width, sample size, and separation in the interquartile range of the distributions of the radar-derived attributes.

Once the observations were binned according the total lightning attributes, the distributions of the radar-derived attributes were examined in each bin. Here, we examine the same radar-derived attributes discussed above (Fig. 11). In these plots, the box gives an estimated range of the radar-derived attribute with 50 percent confidence, and the whiskers give an estimated range of the radar-derived attribute with 90 percent confidence. When the boxes and whiskers in these distributions cover a small range, then this information will be particularly valuable because it can provide a precise estimate of the radar-derived attributes.

There are a few patterns that emerge from these distributions. First of all, there was an expected gradual increase in the radar-derived attributes with increasing Max FED, although it is clear that even when the Max FED was small, there were some occasions in which the radar-derived attributes were quite large. In several cases, the range of 50 percent and 90 percent estimates (i.e., the boxes and whiskers) remained relatively small compared to the overall range of the radar-derived attributes. This was especially true for the distributions of -20MaxRef associated with high levels of Max FED and distributions of ET40 associated with low levels of Max FED. Therefore, the Max FED will likely be particularly useful in predicting -20MaxRef and ET40.

Reversing the above comparison, another potential use of the information presented herein is to estimate total lightning from radar-derived attributes. In particular, using radar-derived attributes to determine if there will or will not be lightning would be valuable in forecasts for outdoor events, where any lightning could trigger an evacuation. With this in mind, rather than examining distributions of the Max FED, probabilities that the Max FED will exceed various thresholds given the value of radar-derived attributes were computed. These probabilities are shown in Fig. 12.

First of all, for all radar-derived attributes other than -20MaxRef, the probability of the Max FED exceeding zero was greater than zero for all levels of the radar-derived attributes. This means that if there was a storm with any pixels greater than 40 dBZ, or any VII, there was a chance for lightning to occur. In the case of -20MaxRef, the probability of lightning occurring became non-zero at 15 dBZ. For each radar-derived attribute, the probability of there being lightning then rose as the radar derived attributes increased. With this information, forecasters will be able to relay probabilistic information to customers, who can make decisions based on the amount of risk that they are willing to take.

There are a few caveats to be aware of when attempting to make predictions of lightning based off of radar-derived attributes, or vice-versa. First, for each radar-derived attribute examined, there was a small percentage of observations in all distributions in which high radar-derived attributes were observed, even when the distributions were associated with low values of the total lightning attributes. This means that there will always be a possibility of high radar-derived attributes occurring with low total lightning attributes. Furthermore, in the case of CompRefGT50 and -10RefGT40, there were also observations with zero or near-zero values of the radar-derived attributes when the total lightning attributes were high. Thus, there will always be a chance of low values of radar-derived attributes occurring, despite high levels of observed total lightning activity. These limitations need to be kept in mind when using this information Further investigation needs to be done to determine the exact method of how this information can be delivered to forecasters. A primary issue is that in an operational setting, using the distributions described above to predict the radar-derived attributes would likely be too cumbersome to be implemented. To be effective, this information should be presented to forecasters in a training setting, in which they will have the time needed to examine the
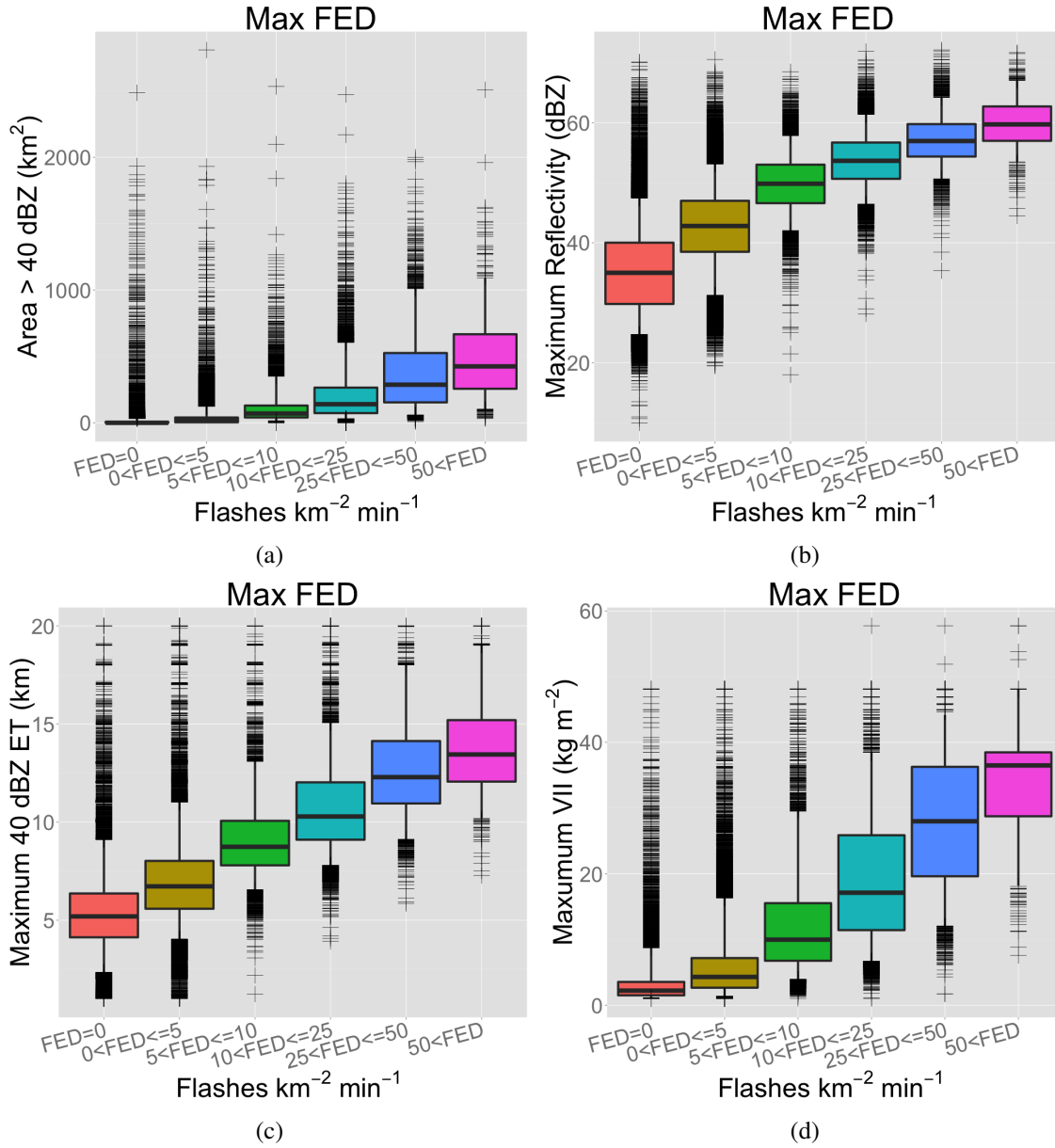
Figure 11: Distributions of the observations of a) Area of reflectivity greater than 40 dBZ at -10 C, b) Maximum reflectivity at -20 C, c) Maximum 40 dBZ ET, and d) Maximum VII binned according to Max FED.
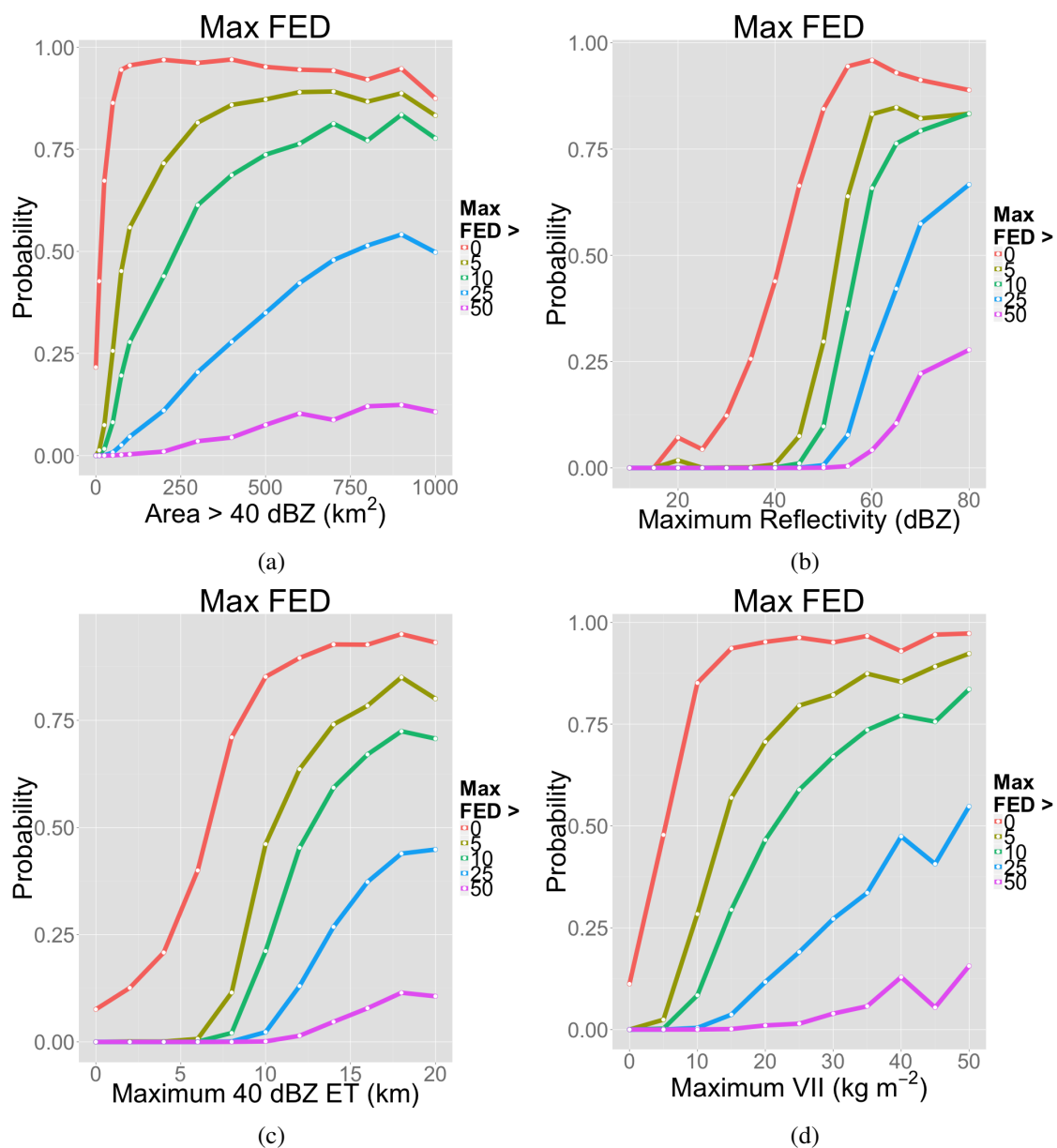
(a)

(b)

(c)

(d)

Figure 12: Max FED exceedance probabilities, given values of: a) Area of reflectivity greater than 40 dBZ at -10 C, b) Maximum reflectivity at -20 C, c) Maximum 40 dBZ ET, and d) Maximum VII.

data in an interactive way. A hands-on training would allow forecasters to enhance their knowledge of the relationships between total lightning and storm intensity, which can in turn be applied in real-time operations.

Hazard Recognition

While there has been relatively little research done in the framework of a climatology examining the total lightning attributes in hazardous and non-hazardous storms, the results of this study compare favorably with case studies done in the domains examined in this study. *Goodman et al.* [2005] showed that in a handful severe thunderstorm detected by the NALMA, the total flash rate was quite large, and maximized at 800 flashes min^{-1} in one case. Additionally, *Bridenstine et al.* [2005] showed the flash rate in an Alabama severe thunderstorm reached nearly 200 flashes min^{-1}. While these flash rates are quite a bit larger than the median and mean flash rates found in severe storms in the NALMA in this study (10 flashes min^{-1} and 35.66 flashes min^{-1}, respectively) they do show that the flash rates in severe storms can be quite a bit larger than in non-severe storms. Similarly, *MacGorman et al.* [1989] observed flash rates maximizing at approximately 14 flashes min^{-1} within 10 km of the mesocyclone in a tornadic Oklahoma thunderstorm. 14 flashes min^{-1} is greater than either the median or mean flash rate found in non-severe storms from the OKLMA in this study (0 and 5.95 flashes min^{-1}, respectively) and is quite similar to the median total flash rate of severe storms in the OKLMA (16 flashes min^{-1}). Finally, *Calhoun et al.* [2013] observed 2 hours of an Oklahoma supercell with a flash rate exceeding 200 flashes min^{-1} at each minute, and maximizing at over 500 flashes min^{-1}. Again, these flash rates are dramatically larger than the median and mean flash rate found in supercell observations from the OKLMA (52 flashes min^{-1} and 64.18 flashes min^{-1}, respectively), but does confirm that hazardous storms can produce prolific amounts of lightning.

As with the relationships between total lightning and radar-derived attributes, the link between total lightning and the production of hazardous weather is likely a storm's updraft. It is a storm's updraft that is primarily responsible for the separation of charge, and storms with strong updrafts (i.e., storms with large updraft volume or updraft mass flux) are capable of separating a large amount of charge, thus producing substantial amounts of lightning [e.g., *Dye et al.*, 1986; *Boccippio et al.*, 2002; *Calhoun et al.*, 2013]. The updraft in hazardous storms (i.e., storms that are supercells or produce severe weather) is typically stronger than in non-hazardous storms [e.g., *Moller et al.*, 1994; *Kain et al.*, 2003]. Therefore, it follows that storms with strong updrafts will likely produce large amounts of lightning and also have a higher probability to produce hazardous weather than storms with weak updrafts.

CONCLUSIONS

In order quantify and examine the relationships between total lightning information and storm intensity in the framework of a multi-year climatology, total lightning information from the Washington D.C., Northern Alabama, and Central Oklahoma and West Texas lightning mapping arrays was examined over a five year period. Thunderstorms in these domains were automatically identified and tracked in order to provide one minute observations of every storm. The total lighting attributes from these one minute thunderstorm observations were then explored in three ways. First, the climatological characteristics of the total lightning attributes were examined. Next, relationships between the total lighting attributes and better understood radar-derived attributes were explored. Finally, the differences in total lightning attributes in hazardous and non-hazardous thunderstorm observations were analyzed.

The climatological characteristics of the total lightning attributes revealed several patterns. Storms in the OKLMA produced the most total lightning per observation, followed by the storms in the NALMA, and finally, the least amount of total lightning per observation was produced by storms in the DCLMA. Through

permutation testing, these differences in the total lightning information between the domains were shown to be statistically significant, but the differences were relatively small.

Additionally, it was found that the relationships between total lightning and radar-derived attributes were examined in order to contextualize the total lightning attributes in terms of thunderstorm attributes well understood by forecasters. In agreement with previous research, most radar-derived attributes examined displayed a moderate to strong, direct correlation with each of the total lighting attributes. Through the strength of these relationships, it was shown that total lightning and radar-derived attributes can be used to estimate one another, and therefore be of use in the forecasting process.

Finally, total lightning attributes in hazardous and non-hazardous storms were examined to determine if total lightning information can be useful in diagnosing hazardous storms. It was found that in general, hazardous (supercell) storms contained a substantially larger amount of total lightning than the non-hazardous storms. This type of information could be particularly useful in a nowcasting setting, where forecasters could get high temporal resolution updates of storm intensity via total ligtning information.

This is one of the first studies to examine total lightning information in the context of a multi-year climatology. Building upon the findings of past research, several relationships were verified, and multiple new relationships were identified. The information provided herein will allow for the data provided by the GLM to be better understood by forecasters and researchers alike, and therefore will improve the value of the information from the GLM.

References

Benjamin, S. G., et al., An Hourly Assimilation–Forecast Cycle: The RUC, *Mon. Wea. Rev.*, *132*, 495–518, 2004.

Boccippio, D. J., W. J. Koshak, and R. J. Blakeslee, Performance assessment of the optical transient detector and lightning imaging sensor. part i: Predicted diurnal variability, *J. Atmos. Oceanic Technol.*, *19*, 1318–1332, 2002.

Bridenstine, P. V., C. B. Darden, J. Burks, and S. Goodman, The application of total lightning in the warning decision making process, in *Preprints, First Conf. on Meteorological Applications of Lightning Data*, Amer. Meteor. Soc., p. P1.2, San Diego, CA, 2005.

Bruning, E. C., The West Texas LMA, in *GLM Science Team Meeting*, Huntsville, AL, 2012.

Calhoun, K. M., D. R. MacGorman, C. L. Ziegler, and M. I. Biggerstaff, Evolution of lightning activity and storm charge relative to dual-doppler analysis of a high-precipitation supercell storm, *Mon. Wea. Rev.*, p. 130128113744001, 2013.

Carey, L. D., and S. A. Rutledge, A multiparameter radar case study of the microphysical and kinematic evolution of a lightning producing storm, *Meteor. Atmos. Phys.*, *59*, 33–64, 1996.

Darden, C. B., D. J. Nadler, B. C. Carcione, R. J. Blakeslee, G. T. Stano, and D. E. Buechler, Utilizing total lightning information to diagnose convective trends, *Bull. Amer. Meteor. Soc.*, *91*, 167–175, 2010.

Doswell, C. A., and D. W. Burgess, *The Tornado: Its Structure, Dynamics, Prediction, and Hazards*, American Geophysical Union, 1993.

Dye, J. E., J. J. Jones, W. P. Winn, T. A. Cerni, B. Gardiner, D. Lamb, R. L. Pitter, J. Hallett, and C. P. R. Saunders, Early electrification and precipitation development in a small, isolated montana cumulonimbus, *J. Geophys. Res.*, *91*, 1231–1247, 1986.

Easterling, D. R., and P. J. Robinson, The diurnal variation of thunderstorm activity in the united states, *J. Climate Allp. Meteor.*, *24*, 1048–1058, 1985.

Emersic, C., P. L. Heinselman, D. R. MacGorman, and E. C. Bruning, Lightning activity in a hail-producing storm observed with phased-array radar, *Mon. Wea. Rev.*, *139*, 1809–1825, 2011.

Goodman, S., et al., The north alabama lightning mapping array: Recent severe storm observations and future prospects, *Atmos. Res.*, *76*, 423–437, 2005.

Goodman, S. J., and D. R. MacGorman, Cloud-to-ground lightning activity in mesoscale convective complexes, *Mon. Wea. Rev.*, *114*, 2320–2328, 1986.

Goodman, S. J., D. E. Buechler, P. D. Wright, and W. D. Rust, Lightning and precipitation history of a microburst-producing storm, *Geophys. Res. Lett.*, *15*, 1185–1188, 1988.

Goodman, S. J., R. Blakeslee, D. Boccippio, H. Christian, W. Koshak, and W. Petersen, GOES-R lightning mapper (GLM) research and applications risk reduction, in *Preprints, Second Symp.: Toward a Global Earth Observation System of Systems-Future National Operational Environmental Satellite Systems*, Amer. Meteor. Soc., p. 2.2, New Orleans, LA, 2006.

Hobson, A. G. K., V. Lakshmanan, T. M. Smith, and M. Richman, An automated technique to categorize storm type from radar and near-storm environment data, *Atmos. Res.*, *111*, 104–113, 2012.

Jing, Z., and G. Weiner, Two-dimensional dealiasing of doppler velocities, *J. Atmos. Oceanic Technol.*, *10*, 798–808, 1993.

Kain, J. S., M. E. Baldwin, and S. J. Weiss, Parameterized updraft mass flux as a predictor of convective intensity, *Wea. Forecasting*, *18*, 106–116, 2003.

Kelly, L., Donald, J. T. Schaefer, and C. A. Doswell, Climatology of nontornadic severe thunderstorm events in the united states, *Mon. Wea. Rev.*, *113*, 1997–2014, 1985.

Krehbiel, P. R., The DC Lightning Mapping Array, in *Preprints, 3rd Conf. on Meteorological Applications of Lightning Data*, Amer. Meteor. Soc., p. 3.2, New Orleans, LA, 2008.

Krehbiel, P. R., R. J. Thomas, W. Rison, T. Hamlin, J. Harlin, and M. Davis, GPS-based mapping system reveals lightning inside storms, *Eos, Trans. Amer. Geophys. Union*, *81*, 21–25, 2000.

Lakshmanan, V., and T. Smith, Data mining storm attributes from spatial grids, *J. Atmos. Oceanic Technol.*, *26*, 2353–2365, 2009.

Lakshmanan, V., R. Rabin, and V. DeBrunner, Multiscale storm identification and forecast, *Atmos. Res.*, *67*, 367–380, 2003.

Lakshmanan, V., T. Smith, K. Hondl, G. J. Stumpf, and A. Witt, A real-time, three-dimensional, rapidly updating, heterogeneous radar merger technique for reflectivity, velocity, and derived products, *Wea. Forecasting*, *21*, 802–823, 2006.

Lakshmanan, V., A. Fritz, T. Smith, K. Hondl, and G. Stumpf, An automated technique to quality control radar reflectivity data, *J. Appl. Meteor. Climatol.*, *46*, 288–305, 2007a.

Lakshmanan, V., T. Smith, G. Stumpf, and K. Hondl, The Warning Decision Support System–Integrated Information, *Wea. Forecasting*, *22*, 596–612, 2007b.

Lhermitte, R., and P. Krehbiel, Doppler radar and radio observations of thunderstorms, *IEEE Trans. Geosci. Electron.*, *17*, 162–171, 1979.

Lhermitte, R., and E. Williams, Cloud electrification, *Rev. Geophys*, *21*, 984–992, 1983.

Long, M. J., A preliminary climatology of thunderstorm penetrations of the tropopause in the united states, *J. Allp. Meteor.*, *5*, 467–473, 1966.

Lund, N. R., D. R. MacGorman, T. J. Schuur, M. I. Biggerstaff, and W. D. Rust, Relationships between lightning location and polarimetric radar signatures in a small mesoscale convective system, *Mon. Wea. Rev.*, *137*, 4151–4170, 2009.

MacGorman, D. R., D. W. Burgess, V. Mazur, W. D. Rust, W. L. Taylor, and B. C. Johnson, Lightning rates relative to tornadic storm evolution on 22 May 1981, *J. Atmos. Sci.*, *46*, 221–251, 1989.

MacGorman, D. R., et al., TELEX the thunderstorm electrification and lightning experiment, *Bull. Amer. Meteor. Soc.*, *89*, 997–1013, 2008.

Maddox, R. A., Meoscale convective complexes, *Bull. Amer. Meteor. Soc.*, *61*, 1374–1387, 1980.

Makowski, J. A., D. R. MacGorman, M. I. Biggerstaff, and W. H. Beasley, Total lightning characteristics relative to radar and satellite observations of Oklahoma mesoscale convective systems, *Mon. Wea. Rev.*, p. 121129145854009, 2013.

Mansell, E. R., C. L. Ziegler, and D. R. Macgorman, A lightning data assimilation technique for mesoscale forecast models, *Mon. Wea. Rev.*, *135*, 1732–1748, 2007.

Mazur, V., A physical model of lightning initiation on aircraft in thunderstorms, *J. Geophys. Res.*, *94*, 3326–3340, 1989.

Moller, A. R., C. A. Doswell, M. P. Foster, and G. R. Woodall, The operational recognition of supercell thunderstorm

environments and storm structures, *Wea. Forecasting*, *9*, 327–347, 1994.

Petersen, W. A., H. J. Christian, and S. A. Rutledge, TRMM observations of the global relationship between ice water content and lightning, *Geophys. Res. Lett.*, *32*, n/a–n/a, 2005.

Rudlosky, S. D., and H. E. Fuelberg, Documenting storm severity in the mid-atlantic region using lightning and radar information, *Mon. Wea. Rev.*, p. 130128113744001, 2013.

Schultz, C. J., W. A. Petersen, and L. D. Carey, Lightning and severe weather: A comparison between total and cloud-to-ground lightning trends, *Wea. Forecasting*, *26*, 744–755, 2011.

Smith, T., and K. Elmore, The use of radial velocity derivatives to diagnose rotation and divergence, in *Preprints, 11th Conf. on Aviation, Range, and Aerospace*, Amer. Meteor. Soc., p. P5.6, Hyannis, MA, 2004.

Williams, E. R., The tripole structure of thunderstorms, *J. Geophys. Res.*, *94*, 13,151–13,167, 1989.

Williams, E. R., M. E. Weber, and R. E. Orville, The relationship between lightning type and convective state of thunderclouds, *J. Geophys. Res.*, *94*, 13,213–13,220, 1989.

Williams, E. R., Boldi B., Matlin A., Weber M., Hodanish S., Sharp D., Goodman S., Raghavan R., and Buechler D., The behavior of total lightning activity in severe Florida thunderstorms, *Atmos. Res.*, *51*, 245–265, 1999.